processes

MDPI

*Article*

# Titanium(III) Oxide Doped with *meta*-Aminophenol Formaldehyde Magnetic Microspheres: Enhancing Dye Adsorption toward Methyl Violet

**Suriyan Radha [1,*], Paul Christygnanatheeba [1], Karuppiah Nagaraj [2], Saradh Prasad [3], Mohamad Saleh AlSalhi [3], Jeyaraj Vinoth Kumar [4], Prabhakarn Arunachalam [5] and Chelladurai Karuppiah [6,*]**

1 Department of Chemistry, Saiva Bhanu Kshatriya College, Aruppukkottai 626101, Tamil Nadu, India
2 SRICT-Institute of Science & Research, Department of Chemistry, UPL University of Sustainable Technology, Block No. 402, Valia Rd., Vataria, Ankleshwar 393135, Gujarat, India
3 Department of Physics and Astronomy, College of Science, King Saud University, P.O. Box 2455, Riyadh 11451, Saudi Arabia
4 Nano Inspired Laboratory, School of Integrated Technology, Yonsei University (International Campus), Incheon 21983, Republic of Korea
5 Chemistry Department, College of Science, King Saud University, P.O. Box 2455, Riyadh 11451, Saudi Arabia
6 Battery Research Center of Green Energy, Ming Chi University of Technology, New Taipei City 24301, Taiwan
* Correspondence: radhminibava@gmail.com (S.R.); chella1986@mail.mcut.edu.tw (C.K.); Tel.: +91-94-4205-9633 (S.R.)

**Abstract:** The demand to synthesize economical detoxification adsorbents of organic pollutants has been a thriving solicitude for most environmental research aspirants. Here, we synthesized a titanium(III) oxide doped with spherical shaped *meta*-aminophenol formaldehyde magnetic microspheres ($Ti_2O_3$/mAPF MMSs) by the polymerization method of $Ti_2O_3$ nanoparticles with formaldehyde and m-aminophenol. SEM analysis confirmed the synthesized material as crystalline in nature and had ~400–450 nm sized particles. The physical characterization of the $Ti_2O_3$/mAPF MMSs were quantitatively revealed by FTIR spectrum and PXRD in elaboration. The carboxylate frequency and the characteristic apex of the titanium–oxygen bond was found in the FTIR spectrum for $Ti_2O_3$/mAPF derived from $Ti_2O_3$. The PXRD patterns proved that the synthesized magnetic microspheres contained $Ti_2O_3$ nanoparticles. The experimental methods of TGA and DTA confirmed the thermal stability and its composition of $Ti_2O_3$/mAPF MMSs. The kinetic adsorption study for methyl violet was confirmed as first-order kinetics. The present study was to investigate the dye desorption of methyl violet from simulated water samples by using a titanium(III) oxide doped with *meta*-aminophenol formaldehyde magnetic microspheres in an adsorption process.

**Keywords:** $Ti_2O_3$ nanoparticles; *meta*-aminophenol; formaldehyde; methyl violet; magnetic microspheres



**Citation:** Radha, S.; Christygnanatheeba, P.; Nagaraj, K.; Prasad, S.; AlSalhi, M.S.; Kumar, J.V.; Arunachalam, P.; Karuppiah, C. Titanium(III) Oxide Doped with *meta*-Aminophenol Formaldehyde Magnetic Microspheres: Enhancing Dye Adsorption toward Methyl Violet. *Processes* **2023**, *11*, 1250. https://doi.org/10.3390/pr11041250

Academic Editors: Huseyin Tombuloglu and Abdulhadi Baykal

Received: 27 January 2023
Revised: 4 April 2023
Accepted: 10 April 2023
Published: 18 April 2023



## 1. Introduction

The progress of rapid industrialization may bring contaminants into aqueous environments that affect the ecosystem. Methyl violet (MV), cationic dye methylene blue (MB), and the anionic dye methyl orange (MO) are three typical organic dyes in wastewater that mainly come from the food and drug industries, and result in negative effects [1–3]. Therefore, it is urgent to find strategies for the fast and efficient removal of organic dyes. Several methods have been reported such as adsorbent materials and chemical catalysis that treat industrial wastewater, but there are some problems in the most common method such as a slow process, secondary pollutants, and regeneration costs, etc. [4]. To solve this problem, many novel photo catalyst methods of dye removal have been created, and they have played an important role in the removal of organic dyes [5,6]. In the recent past, the catalytic potency of coinage metals at the nanoscale has attracted much attention, and leads to weak catalysis and low cycling properties in cyclic performance due to strong

aggregation. Hence, we developed a suitable method to prevent such aggregation and to increase the catalytic activity of coinage metal nanoparticles. Based on this requirement, titanium oxide nanoparticles and titanium oxide based magnetic microspheres on various solid carriers are becoming more popular due to advantages such as dye degradation without producing secondary pollutants, and the degraded products are eco-friendly with biological systems. Additionally, titanium oxide based magnetic microspheres and large numbers of reports such as MOFs and PET have been reported on their carriers to enhance their dispersion, catalytic activity, and cycling stability.

Titanium oxide based magnetic microspheres have been attracting much attention due to their dye adsorption property. Synthetic cationic and anionic dyes like methyl violet and EBT substances are usually colored and are difficult to biodegrade because of their mosaic and synthetic structures of an aromatic compound [7–11]. The production of a commercial dye is a major source of the large number of effluent deterioration due to the byproduct of industrial pollution [12,13]. Moreover, the defilement leads to mutagenic and carcinogenic effects because of both the surface and groundwater hazards, which are particularly used in anionic dyes [3,14]. Anionic dyes based on a metal complex and reactive dyes are problematic to degrade because they can resist heat and microbial attack [15]. Therefore, methyl violet dyes need to be eliminated from industrial effluent by various treatment technologies such as advanced oxidation processes (AOPs), solvent extraction, precipitation, and photo catalytic degradation [16–20]. Due to the use of industrial organic dyes to supply the constant growth in people's living standards, they have become of high concern because their byproducts lead to serious human health issues because of their highly toxic products [21–24]. An adsorption technique is easy to handle; in particular, low cost resin-based phenolic materials and agricultural wastes, especially resin-based phenolic materials, have very good properties such as low toxicity, outstanding biocompatibility, and porosity [23–29]. They have a well-to-do array of patterns (e.g., graphitized flakes and nanofibers) [29–33]. In all of these, colloidal resin microspheres are gaining significant attention due to a variety of applications in particle templates, colloidal assemblies, biomedical fields, and optical sensing [9,28–32].

The interesting new catalytic, electronic, optical, and biocompatible properties of colloidal resin microsphere-based nanocomposites have moved forceful research over the past decades. In particular, amine group-attached magnetic particles have a wide variety of applications in drug delivery, catalysis, and enzyme immobilization [34–37]. In the last two decades, much attention has focused on various phenolic-formaldehyde resins such as 3-aminophenol-formaldehyde resin and resorcinol-formaldehyde resin because phenolic resins exhibit a strong stickiness due to their mussel-like properties [38–42]. For instance, the catalytic effect of resorcinol-formaldehyde-hybridized nanogold for MB [43–46] and the development of phenolic-formaldehyde resin nanomaterials are of great scientific significance and practical application value. Recently, magnetic core-shell composites have attracted a great deal of attention for their good magnetic responsibility and can be easily magnetized. These microspheres are an essential catalytic property in the advancement of photocatalysis, batteries, and gas storage, which tune the material properties. A microsphere magnetic particle [47–50] is a fascinating design to use as a microsphere material to enhance the nanoparticles' stability, dispersion as well as protect microsphere materials and develop microsphere magnetic materials [51–54].

Over the past few years, the research has focused on phenolic-formaldehyde resin (PF resin)- and resorcinol-formaldehyde resin (RF resin)-based magnetic microspheres due to the progressive development of implications and the applications of magnetic microspheres. The synthesis of various types of PF resins such as phenoplasts has been progressively reported due to their mussel-like properties, [55,56]. For instance, Gavina et al. [57] studied the catalytic effect of RF resin-nano gold hybridized for methyl blue. The significant advancement of RF resins as a nanomaterial and added a value of practical application. Furthermore, mussel chemistry involving catechol groups can adhere to a variety of organic and inorganic composites with various structures that can be fabricated by combining

organic and inorganic materials with phenolic-formaldehyde resins. Methyl violet is an eminent organic dye commonly used by industries concerned in the rubber, pharmaceutical, cosmetics, textile, plastics, leather, paper, pharmaceutical, and food industries. Colored wastewater lacking correct action can profusely cause trouble such as the chemical oxygen demand in the water body and expansion in toxicity [58–60]. Dyes have mainly been reported to be directly connected to human diseases such as hyperbilirubinemia, amyloidosis, and anemia [61–63]. Nowadays, the most extensively used methods for the elimination of colored dyes from dye-rich wastewater are physicochemical (e.g., photo catalytic degradation, ultra-filtration, and physical adsorption on activated carbon). In recent years, activated carbon prepared from agricultural wastes/byproducts have been used as adsorbents for the removal of dyes as an alternative to commercial activated carbon. These methods are attractive given their high effectiveness, but are difficult and exclusive [64–72]. A recent study investigated nanocomposites consisting of a magnetite core and an outer Ag-decorated anatase shell and their application for the visible-light photodegradation of cationic and anionic dyes [73–76]. As research develops, more high attainment MNP hybrids may stimulate various new fields of environmental monitoring, bio-catalysis, and bio-detection applications [77–80].

In the present study, we report on the preparation of titanium(III) oxide doped with spherical shaped *meta*-aminophenol formaldehyde magnetic microspheres ($Ti_2O_3$/mAPF MMSs) by in situ polymerization in an aqueous solution. We believe that the present results of $Ti_2O_3$/mAPF MMSs is an inexpensive and eco-friendly option and can be used as an effective adsorbent for the removal of methyl violet from an industrial effluent. These microspheres will efficiently take out methyl violet. The as prepared $Ti_2O_3$/mAPF MMSs had large clusters of $NH_2$ groups over the surface, allowing for its unique potential and applicability.

## 2. Experimental Method

### 2.1. Materials

*meta*-Aminophenol ($C_6H_7NO$), methylene oxide ($CH_2O$), titanium tetrabutoxide ($Ti(C_4H_9O)_4$), polyethylene oxide 600 ($H(OCH_2CH_2)_nOH$), aqueous ammonia ($NH_4OH$), methyl violet ($C_{24}H_{28}N_3Cl$), and ethanol ($C_2H_5OH$) ($\geq$99.8%) were purchased from Sigma Aldrich, St. Louis, MO, USA.

### 2.2. Preparation of Titanium(III) Oxide Nanoparticles

Prior to synthesis, $Ti(C_4H_9O)_4$ (6 mL) was poured with 1 mL of anhydrous $C_2H_6O$ in a round bottom flask (RBF) and maintained in a water bath (thermostat-controlled) at 50 °C. Then, 2.5 mL of PEG-600 was added drop by drop in the direction of the RBF and the mixture was stirred for 3 h to obtain a brightness sol. Finally, the brightness sol was dried with the help of a vacuum oven at 120 °C for 24 h to obtain a gel (yellow color). The hybrid polyethylene oxide 600-based gel was in a porcelain boat, maintained at RT (high pure argon flow) for 30 min, and in a quartz tube in a controlled atmosphere furnace (heated at 5 °C $min^{-1}$) at 1200 or 1500 °C for 6 h. Finally, reduced black oxides were ground into regular powders [81].

### 2.3. Synthesis of $Ti_2O_3$/mAPF MMSs

The *meta*-aminophenol-formaldehyde-based microspheres (mAPF) were prepared with a slight modification as per the previous literature [82]. In this synthetic procedure, 0.33 g of *meta*-aminophenol was added into 52 mL of $C_2H_5OH$ and 20 mL of $H_2O$, afterward, 224 µL of an aqueous solution ($NH_4OH$,) of $NH_3$ was added to form a consistent solution for 30 min at 40 °C after the addition of 180 µL of the $CH_2O$ solution. The obtained solution was stirred at 60 °C for 300 min and then heated at 120 °C for 24 h (Teflon-lined autoclave, Shilpa Enterprises, Bengaluru, India). The resin spheres were purified with double-distilled (DD) water and $C_2H_5OH$ by centrifugation at a speed of 6000 rpm. The

synthesized precipitates (mAPF microspheres) and $Ti_2O_3$ nanoparticles were ultrasonicated in 10 mL of DD $H_2O$ for 3 h.

## 3. Results and Discussion

Spherical shaped $Ti_2O_3$/mAPF MMSs were synthesized by a sol–gel polycondensation method in dihydrogen monoxide. The measured procedure of $Ti_2O_3$/mAPF MMSs and the mechanism for the formation of *meta*-aminophenol-formaldehyde microparticles is shown in Scheme 1.

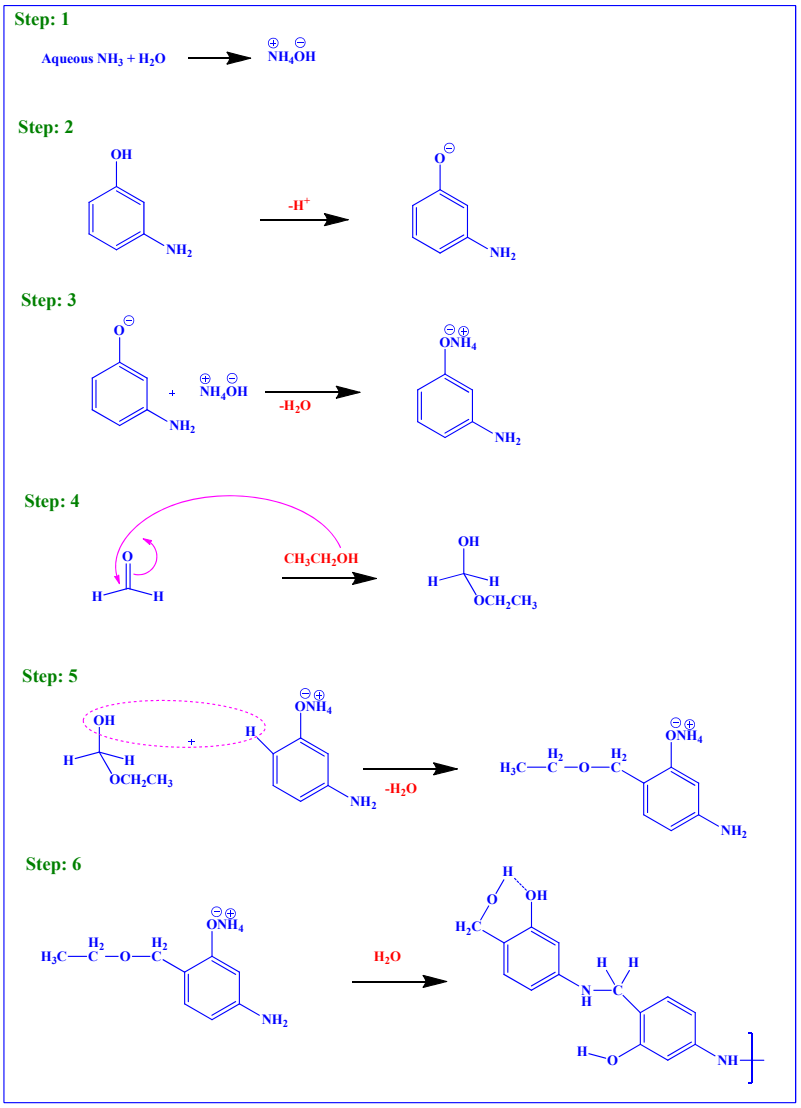


**Scheme 1.** Plausible mechanism for the formation of $Ti_2O_3$/mAPF MMSs.

### 3.1. Characterization

The as-synthesized mAPFR MMSs were examined by scanning electron microscopy (SEM). Figure 1A shows that the SEM images of the as synthesized MMSs (a) and $Ti_2O_3$/mAPF MMSs (b) contained a number of MMSs. The magnified SEM image of these MMSs demonstrates that the mAPFR MMSs were in the diameter of ca. ~400–450 nm. Additionally, Figure 1A(a) reveals that the MMSs had an even spherical shape and that particles did not accumulate. The SEM image of $Ti_2O_3$ decorated on the mAPFR MMSs is shown in Figure 1A(b).

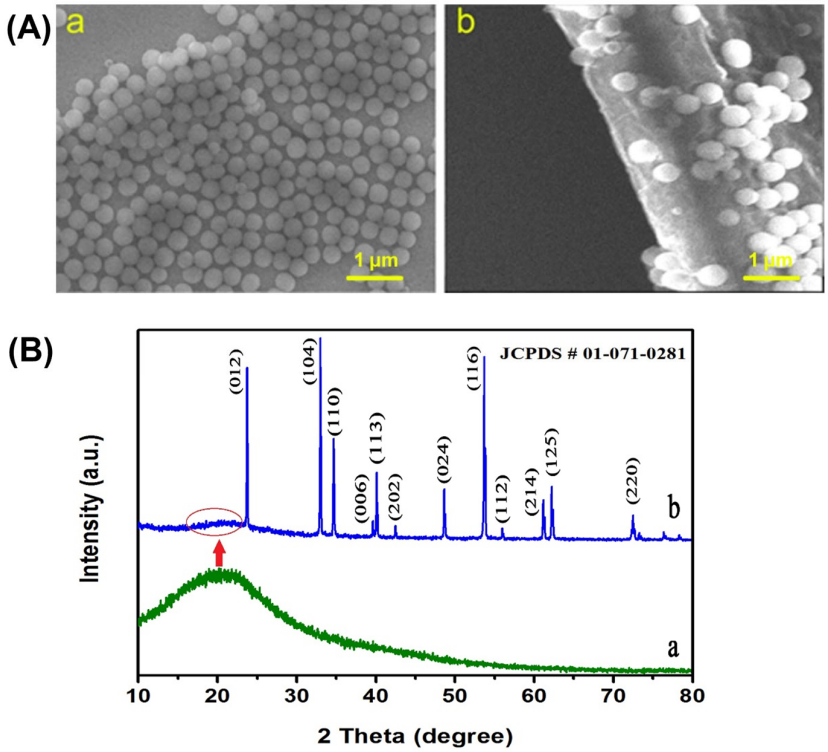


**Figure 1.** (**A**) SEM images for (**a**) mAPF and (**b**) $Ti_2O_3$/mAPF MMSs. (**B**) PXRD of (**a**) mAPF MMSs, (**b**) $Ti_2O_3$/mAPF MMSs.

Figure 1B shows the PXRD studies of the (a) mAPF MMS and (b) $Ti_2O_3$/mAPF MMS samples. Typically, the PXRD pattern for the mAPF MMSs shows a broad line parallel to the amorphous nature of mAPF, which appeared at a 2θ value of 20–30°, and the $Ti_2O_3$ diffraction patterns indexed to (2θ = 3.73 (012), 2.70 (104), 2.57 (110), 2.27 (006), 2.24 (113), 2.12 (202), 1.86 (024), 1.70 (116), 1.50 (122), 1.50 (214), 1.48 (125), 1.30 (220), 1.29 (036) and 1.24 (312) are practical in the 10–80° 2θ range. All the peaks were referenced according to the JCPDS cards (JCPDS # 01-071-0281). The occurrence of all peak intensities according to the JCPDS cards suggests a rhombohedral (R-3c space group) structure. The PXRD patterns proved that the synthesized magnetic microspheres contained a $Ti_2O_3$ stable phase and remained unchanged during the synthetic methodology. After doping the $Ti_2O_3$ nanoparticles with mAPF, the intensities of the PXRD diffraction lines of mAPF decreased [82]. Using Debye Scherrer's equation $D = K\lambda/\beta_{hkl} \cos\theta$, the crystalline size of the $Ti_2O_3$ was around ~100 nm.

Figure 2 shows the FTIR spectrum of the pristine mAPF and $Ti_2O_3$ compared to the $Ti_2O_3$/mAPF MMSs. As seen from Figure 2a, the peak at 1289 $cm^{-1}$ formed from the aromatic-oxygen–carbon stretching; at the same time, the broad band at 1379 $cm^{-1}$ can be associated with the carbon–nitrogen from the $NH_2$ group [83]. The arrival of a low and broad peak at 3372 $cm^{-1}$ and a strong and narrow peak at 1613 $cm^{-1}$ were accredited to the occurrence of the –OH and $NH_2$ groups, respectively. The appearance of a peak around 1500 $cm^{-1}$ was attributed to the carbon–hydrogen stretching, considering that the absorption band around 2900 $cm^{-1}$ was because of the methylene asymmetric stretching vibration. For the $Ti_2O_3$ magnetic nanoparticles (Figure 2b), the peak that appeared at 526 $cm^{-1}$ was responsible for the titanium–oxygen bonds. The symmetric (1578 $cm^{-1}$) and asymmetric vibrations (1634 $cm^{-1}$) of the carboxylate groups derived from ligands on the surface $Ti_2O_3$. Figure 2c reveals the spectra of the $Ti_2O_3$/mAPF MMS composites. The carboxylate groups appeared at 1500 $cm^{-1}$, and the respective apex of the titanium–oxygen bond that appeared around 476, 534 $cm^{-1}$ in the FTIR of $Ti_2O_3$/mAPF was adopted from $Ti_2O_3$. The rest of the bands originated from mAPF along with the stretching vibrations at

3252 $cm^{-1}$ (oxygen–hydrogen or –OH . . . nitrogen), 3366 $cm^{-1}$ (N-H or NH . . . O), Ar–H vibration (1212 $cm^{-1}$), and the respective aromatic rings bands around 1517 $cm^{-1}$ [84–88].

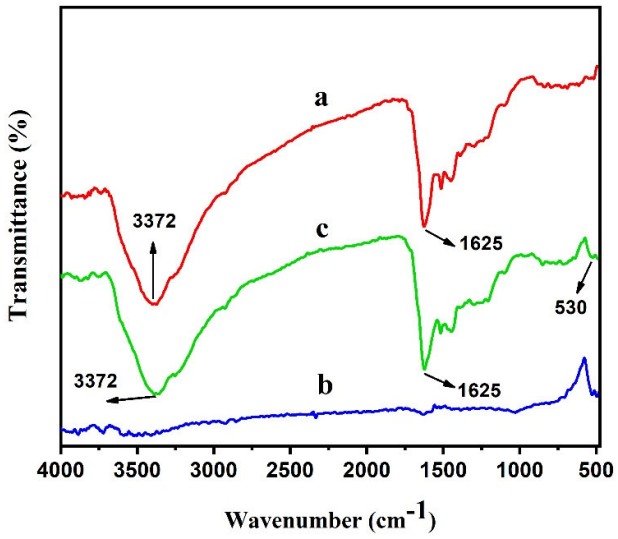


**Figure 2.** FTIR spectra of (**a**) mAPF, (**b**) $Ti_2O_3$ and (**c**) $Ti_2O_3$/mAPF MMS.

Thermogravimetric analysis (TGA) of the *meta*-aminophenol-formaldehyde-based microspheres was carried out using a Mettler Toledo, TGA/DSC 1 series apparatus and conducted at a heating rate of 10 °C $min^{-1}$ under a constant flow of nitrogen to determine the calcination temperature. The *meta*-aminophenol-formaldehyde-based microspheres (mAPF) were investigated using an X-ray diffractometer (Desktop X-ray) and recorded using $CuK_\alpha$ ($\lambda$ = 1.54056 Å) radiation operated at 40 kV and 30 mA. The mAPF was characterized and recorded using Fourier transform infrared spectroscopy (FTIR, Bruker IFS28) to analyze and detect the functional group at the scanning region of 4000–400 $cm^{-1}$. Figure 3 shows the composition and thermal stability of the $Ti_2O_3$/mAPF MMSs supplementally described by a thermogravimetric analyzer. The sample was heated from room temperature to 900 °C. The sample weights of the $Ti_2O_3$ and $Ti_2O_3$/mAPF MMSs were 13.6 and 15.2 mg, respectively. The $Ti_2O_3$/mAPF MMS decayed in two stages (Figure 3, blue line). The initial weight loss to 100 °C was equivalent to the evaporation of the solvent and dihydrogen monoxide. Second, 39% weight loss occurred upon increasing the heat from 245 to 577 °C. During this time, the mAPF deliberately abstracted due to the eradication of sundry compounds along with water, $H_2$, $CH_4$, $NH_3$, carbon dioxide, carbon monoxide, ethane, and some truncated hydrocarbons.

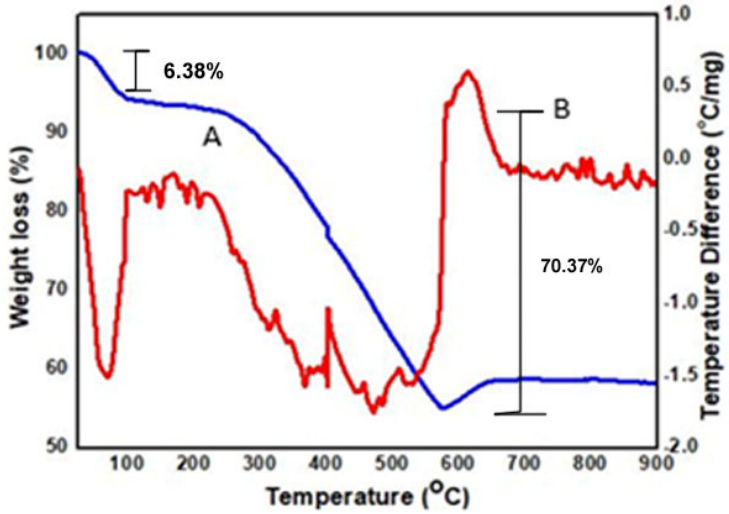


**Figure 3.** TGA curve of $Ti_2O_3$/mAPF (blue line—**A**) and the DTA curve of $Ti_2O_3$/mAPF (red line—**B**).

The obtained $Ti_2O_3$/mAPF MMSs were predicted to absorb organic dyes displaying $NH_2$ and OH groups, since they have distinct functional groups with similar surface polarity (e.g., $NH_2$, OH, OH-$CH_3$, etc.). In the present report, methyl violet was removed to analyze the adsorption potential of $Ti_2O_3$/mAPF MMSs. As shown in Figure 4A, the color of methyl violet disappeared after the integration of $Ti_2O_3$/mAPF MMSs because of the adsorption of methyl violet onto the $Ti_2O_3$/mAPF MMSs. Figure 4A shows the UV–Vis spectra of the methyl violet adsorption by the $Ti_2O_3$/mAPF MMSs at various time (0, 6, 12, 18, 24, 30, 36, 42, 48, and 60 min) intervals. Methyl violet was adsorbed on the surface of the $Ti_2O_3$/mAPF MMSs via conjugated л bonding and hydrogen bonding.

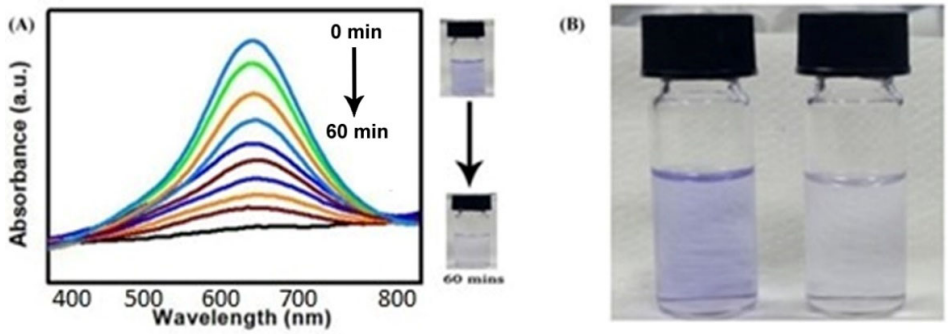


**Figure 4.** (**A**) UV−Vis spectra of methyl violet adsorption by the $Ti_2O_3$/mAPF MMSs at various time intervals. (**B**) The corresponding photographic image of dye degradation.

### *3.2. Adsorption Isotherm*

Adsorption isotherms are of extensive research importance to primary methods of adsorption techniques that are used to predict the adsorption capacity of a given material (e.g., the Langmuir and Freundlich isotherms). Adsorption isotherms can be employed to resolve the greatest use of adsorbents and to design a system of adsorption for the removal of a dye from its solution, in order to provide an appropriate correlation for the equilibrium curve [89]. The interrelationship of Langmuir and Freundlich isotherms are shown in Table 1. The value of $R_L$ indicates the shape of the isotherms to be either unfavorable ($R_L > 1$), linear ($R_L = 1$), favorable ($0 < R_L < 1$), or irreversible ($R_L = 0$) [90]. In these cases, an $R_L$ value less than 1 indicates that adsorption is favorable. Another Langmuir constant, $Q_0$, indicates the adsorption capacity. During this study, the value of $R_L$ was found to be 0.007 ($Ti_2O_3$) and 0.003 ($Ti_2O_3$/mAPF MMS), suggesting that methyl violet adsorption on both was favorable for $Ti_2O_3$ and $Ti_2O_3$/mAPF MMSs. Furthermore, the value of the Freundlich isotherm slope was found to be 0.506 ($Ti_2O_3$) and 0.096 ($Ti_2O_3$/mAPF MMS), suggesting that a large amount of methyl violet was adsorbed by $Ti_2O_3$ and $Ti_2O_3$/mAPF MMSs. A comparison of the previous studies of different dyes adsorbed on various bio adsorbents and methyl violet/EBT adsorbed on different adsorbents is given in Tables 2 and 3 [82–90]. As seen from Tables 2 and 3, the $Ti_2O_3$/mAPF MMSs had a moderate catalytic performance with the degradation of cationic dye, suggesting that $Ti_2O_3$/mAPF MMSs have an excellent application compared to other adsorbents.

**Table 1.** The results of various adsorption isotherms.

| Isotherm | $Ti_2O_3$/mAPF MMS | $Ti_2O_3$ |
|---|---|---|
| | $-x/m = k.P^{1/n}$ | |
| Slope (1/n) | 0.096 | 0.506 |
| Intercept (log k) | 1.973 | 0.350 |
| Correlation coefficient (r) | 0.939 | 0.990 |
| | **Langmuir (xm = aP1 + bP)** | |
| Intercept (1/ $Q_0$b) | 0.006 | 0.613 |
| Correlation coefficient (r) | 0.999 | 0.994 |
| $Q_0$ (mg $g^{-1}$) | 132.62 | 13.94 |
| b (L $mg^{-1}$) | 0.795 | 8.571 |
| $R_L$ | 0.003 | 0.007 |

**Table 2.** Different types of adsorbents used for the decontamination of different dyes.

| S. No | Adsorbent | Dyes | $Q_0$ (mg $g^{-1}$) |
|---|---|---|---|
| 1 | Sodium carbonate—Treated B Vulgaris | BG | 40.12 |
| 2 | Hydrochloric acid—Treated Bambusa | BG | 32.15 |
| 3 | Dialectical Behavior Therapy—Treated B Vulgaris | BG | 31.02 |
| 4 | Coconut fiber | Congo Red | 2.80 |
| 5 | Musa sapientum | BB9 | 19.90 |
| 6 | orange zest | Acid Violet | 19.50 |
| 7 | stalks of grasses | BB9 | 19.80 |
| 8 | Sugarcane megass | Acid Orange 10 | 5.97 |
| 9 | Phoenix dactylifera (kernels) | BB9 | 16.80 |
| 10 | Coconut fiber | Direct red 28 | 6.70 |
| 11 | Citrullus lanatus | Crystal Violet | 11.90 |
| 12 | Coal-based adsorbent | Direct brown 1 | 5.90 |
| 13 | Rice hull | BB9 | 19.50 |
| 14 | Cobnuts or filberts | BB9 | 8.80 |
| 15 | Live oaks | BG | 2.08 |
| 16 | Rice hull ash | BG | 24.13 |
| 17 | Saraca asoca | BG | 123.0 |
| 18 | Rice straw | BG | 113.10 |
| 19 | SCBA | BG | 118.17 |
| 20 | Native Allium sativum | EBT | 100.22 |
| 21 | Washed Allium sativum | EBT | 89.40 |
| 22 | $Ti_2O_3$/mAPF MMSs (this Study) | Methyl Violet | 132.62 |

EBT = Eriochrome Black T; BG = Brilliant Green; BB9 = Basic Blue 9.

**Table 3.** Comparative study of the $Ti_2O_3$/mAPF MMSs vs. different adsorbents.

| S. No | Adsorbent Detail | $Q_0$ (mg $g^{-1}$) |
|---|---|---|
| 1 | Graphite | 101.02 |
| 2 | Acid-modified Graphite | 69.39 |
| 3 | Native pyrena | 6.8 |
| 4 | Cold plasma treated-pyrena shells | 19.08 |
| 5 | Microwave treated-pyrena shells | 30.38 |
| 5 | Magnetite/silica/pectinNPs | 66.28 |
| 6 | Ponded ash | 95.87 |
| 7 | Phosphoric acid -modified berry cultivation | 132.04 |
| 8 | Nickel ferrite@NPs | 82.41 |
| 9 | Nickel ferrite magnetic NPs | 48.2 |
| 10 | $C_{12}H_{20}N_2O_5$ (Hydrophobic cross-linked) | 16.3 |
| 11 | β-CD | 21.4 |
| 12 | Nickel–iron alloy-hydroxides | 132.4 |
| 13 | Sweet lime-activated carbon | 47.43 |
| 14 | Smectite clay composite | 3.50 |
| 15 | China clay/polymer | 0.56 |
| 16 | Steatite or soapstone | 2.15 |
| 17 | Hydrochloric acid modified clay | 17.18 |
| 18 | Sulfuric acid modified clay | 17.48 |
| 19 | $Al_2H_2O_{12}Si_4$ (Gelwhite L. Bentolite.) | 100.5 |
| 20 | Stringybark | 53.25 |
| 21 | Native Allium sativum | 99.52 |
| 22 | Washed Allium sativum | 89.40 |
| 23 | $Ti_2O_3$/mAPF MMS (This Study) | 132.62 |

### *3.3. Kinetics of Adsorption Study*

Kinetics of adsorption was used to understand the pathway of adsorption of methyl violet upon the $Ti_2O_3$/mAPF MMSs. It was noted that the organic dye degradation primarily followed first-order reaction kinetics [91–95]. The experimental data results were

fitted into a first-order model for the adsorption of methyl violet onto $Ti_2O_3$/mAPF MMSs. The results of the kinetics of the adsorption of methyl violet on $Ti_2O_3$/mAPF MMSs are shown in Table 4. It can be seen that the first-order model fit better than the pseudo-first-order model, with a value of $R^2 = 0.999$ for the $Ti_2O_3$/mAPF MMSs. Similarly, the calculated $q_e$ value fit very well with the experimental data. The results suggest that the degradation of methyl violet over $Ti_2O_3$/mAPF MMSs can be described by the first-order reaction of kinetic ln ($C_i/C_t$) = kt, where k is the rate constant ($h^{-1}$), $C_i$ is the initial concentration, and $C_t$ is the dye concentration at time. Linear correlations are important, as evidenced from the value of 'r'. This indicates the applicability of these kinetic equations and the first-order of the adsorption process.

**Table 4.** Experimental evidence for the studies of the kinetics of the adsorption of methyl violet on $Ti_2O_3$/mAPF MMSs.

| Time (min) | Log ($C_i/C_t$) | 5 + Log [1 − U (t)] | 2 + Log ($q_e - q_t$) |
|---|---|---|---|
| 10 | 0.61 | 4.32 | 2.29 |
| 20 | 0.64 | 4.27 | 2.24 |
| 30 | 0.83 | 4.00 | 1.98 |
| 40 | 0.85 | 3.95 | 1.96 |
| 50 | 1.02 | 3.69 | 1.66 |
| 60 | 1.07 | 3.27 | 1.23 |

### *3.4. Activation Parameters*

The Van't Hoff equation [96,97] gives the relationship between the standard Gibbs free energy change and the equilibrium constant. It is expressed as follows:

$$\text{Gibbs free energy change} = -RT \ln \text{equilibrium constant reaction for adsorption} \quad (1)$$

$$\text{Gibbs free energy change} = \text{enthalpy of activation} - T \times \text{entropy of activation} \quad (2)$$

The activation parameters affecting the methyl violet adsorption on $Ti_2O_3$/mAPF MMSs and $Ti_2O_3$ are shown in Table 5.

**Table 5.** The thermodynamic activation parameters for the methyl violet adsorption.

| Adsorbent | Temp (K) | $K_L$ | $\Delta G^\circ$ KJ $mol^{-1}$ | $\Delta G^\circ$ KJ $mol^{-1}$ | $\Delta S^\circ$ $JK^{-1}$ $mol^{-1}$ | $R^2$ |
|---|---|---|---|---|---|---|
| **$Ti_2O_3$/mAPF MMS** | 293 | 2.380 | −2.112 | 2.433 | 15.480 | 0.989 |
| | 298 | 2.412 | −2.180 | | | |
| | 303 | 2.445 | −2.247 | | | |
| | 308 | 2.483 | −2.326 | | | |
| | 313 | 2.536 | −2.415 | | | |
| | 318 | 2.565 | −2.485 | | | |
| **$Ti_2O_3$** | 293 | 2.031 | −1.716 | 2.272 | 13.665 | 0.944 |
| | 298 | 2.052 | −1.780 | | | |
| | 303 | 2.130 | −1.904 | | | |
| | 308 | 2.155 | −1.936 | | | |
| | 313 | 2.187 | −1.998 | | | |
| | 318 | 2.218 | −2.068 | | | |

The Gibbs free energy change was calculated using Equation (1) where the entropy and enthalpy of activation was calculated from the slope and intercept of lnK vs. 1/T. As seen from Table 5, at all temperatures (20 to 45 °C) for both $Ti_2O_3$/mAPF MMSs and $Ti_2O_3$, the Gibbs free energy change was negative, suggesting a spontaneous and favorable adsorption process that also decreased with an increase in temperature, which shows the endothermic reaction of adsorption [98,99]. In addition, the adsorption of methyl

violet is a physically controlled process that indicates that $\Delta G^{\circ}$ fell in the region of −20 to 0 KJ $mol^{-1}$ [100]. Hence, based on the Mattson criteria [40], we can safely assume that the adsorption of methyl violet onto $Ti_2O_3$/mAPF MMSs and $Ti_2O_3$ is a physical process, and that it may involve physical forces such dipole and/or hydrogen bonding forces. The positive enthalpy of activation (2.383 KJ $mol^{-1}$ ($Ti_2O_3$/mAPF MMS) and 2.168 KJ $mol^{-1}$ ($Ti_2O_3$) suggests an endothermic adsorption process in both cases. The positive entropy of activation (15.39 $JK^{-1}$ $mol^{-1}$ ($Ti_2O_3$/mAPF MMS) and 13.55 $JK^{-1}$ $mol^{-1}$ ($Ti_2O_3$)) suggests an increase in temperature assisted in dye adsorption by the removal of $H_2O$ molecules from the surface of the $Ti_2O_3$/mAPF MMSs [88,101,102].

### *3.5. Desorption Studies*

In the present desorption study, we used various solutions of pH 9, 10, 11, and 12 to desorb methyl violet adsorbed on the $Ti_2O_3$/mAPF MMSs. Ours result suggest a lower adsorption at higher pH. When increasing the pH from pH 9 to pH 12, the desorption of methyl violet increased from 21.95 to 43.13%, indicating an increased repulsion between the adsorption sites and methyl violet molecules. The moderate desorption efficiency of the $Ti_2O_3$/mAPF MMSs suggests that the interactions between the methyl violet molecules and the $Ti_2O_3$/mAPF MMSs were via conjugated л bonding and hydrogen bonding.

## 4. Conclusions

The present investigation dealt with the removal of the organic dye methyl violet on $Ti_2O_3$/mAPF MMSs. Adsorption isotherms and kinetic studies of the $Ti_2O_3$/mAPF MMSs are shown first order of adsorption process. The desorption of methyl violet increased with a decrease in the concentration and particle size. With an increase in the contact time and amount of the adsorbent, the percentage removal increased. The $Ti_2O_3$/mAPF MMSs improved the actual adsorption in the elimination of crystal violet; successful dye decolorization was attained within 60 min. The experimental data confirm the first-order kinetics for the $Ti_2O_3$/mAPF MMS samples. $Ti_2O_3$/mAPF MMSs showed a good catalytic performance with the degradation of methyl violet, indicating that $Ti_2O_3$/mAPF MMSs have an excellent application in environmental protection. It can be concluded from these results that $Ti_2O_3$/mAPF MMSs are the best adsorption method for the removal of methyl violet from an industrial effluent.

**Author Contributions:** Conceptualization, Methodology, Formal analysis, Investigation, Resources, Writing—original draft, Project administration, S.R.; Validation, Investigation, Writing—review & editing, P.C.; Writing—review & editing, K.N.; Visualization, S.P.; Funding acquisition, Writing—review & editing, M.S.A.; Validation, Writing—review & editing, J.V.K.; Writing—review & editing, P.A.; Supervision, Writing—review & editing, C.K. All authors have read and agreed to the published version of the manuscript.

**Funding:** The authors express their sincere appreciation to the Researchers Supporting Project number (RSPD2023R723) at King Saud University, Riyadh, Saudi Arabia.

**Data Availability Statement:** Not applicable.

**Conflicts of Interest:** The authors declare they have no known competing financial interest or personal relationships that could have appeared to influence the work reported in this paper.

## References

1. Gupta, N.; Singh, H.P.; Sharma, R.K. Metal nanoparticles with high catalytic activity in degradation of methyl orange: An electron relay effect. *J. Mol. Catal. A Chem.* **2011**, *335*, 248–252. [CrossRef]
2. Dong, Y.; Liu, T.; Sun, S.; Chang, X.; Guo, N. Preparation and characterization of $SiO_2$/polydopamine/Ag nanocomposites with long-term antibacterial activity. *Ceram. Int.* **2014**, *40*, 5605–5609. [CrossRef]
3. Yang, Y.; Ji, H.; Duan, H.; Fu, Y.; Xia, S.; Lu, C. Controllable synthesis of mussel-inspired catechol-formaldehyde resin microspheres and their silver-based nanohybrids for catalytic and antibacterial applications. *Polym. Chem.* **2019**, *10*, 4537–4550. [CrossRef]

4. Greczynski, G.; Hultman, L. Reliable determination of chemical state in X-ray photoelectron spectroscopy based on sample-work-function referencing to adventitious carbon: Resolving the myth of apparent constant binding energy of the C 1s peak. *Appl. Surf. Sci.* **2018**, *451*, 99–103. [CrossRef]
5. Gong, C.; Li, Q.; Zhou, H.; Liu, R. Tiny Au satellites decorated $Fe_3O_4$@3-aminophenol-formaldehyde core-shell nanoparticles: Easy synthesis and comparison in catalytic reduction for cationic and anionic dyes. *Colloids. Surf. A Physicochem. Eng. Asp.* **2018**, *540*, 67–72. [CrossRef]
6. Gong, C.; Zhou, Z.; Li, J.; Zhou, H.; Liu, R. Facile synthesis of ultra stable $Fe_3O_4$@Carbon core-shell nanoparticles entrapped satellite au catalysts with enhanced 4-nitrophenol reduction property. *J. Taiwan. Inst. Chem. Eng.* **2018**, *84*, 229–235. [CrossRef]
7. Alprol, A.; Heneash, A.; Ashour, M.; Abualnaja, K.; Alhashmialameer, D.; Mansour, A.; Sharawy, Z.; Abu-Saied, M.; Abomohra, A. Potential Applications of *Arthrospira platensis* Lipid-Free Biomass in Bioremediation of Organic Dye from Industrial Textile Effluents and Its Influence on Marine Rotifer (*Brachionus plicatilis*). *Materials* **2021**, *14*, 4446. [CrossRef]
8. Gong, R.; Li, M.; Yang, C.; Sun, Y.; Chen, J. Removal of cationic dyes from aqueous solution by adsorption on peanut hull. *J. Hazard. Mater.* **2005**, *121*, 247–250. [CrossRef]
9. Barka, N.; Abdennouri, M.; EL Makhfouk, M. Removal of Methylene Blue and Eriochrome Black T from aqueous solutions by biosorption on *Scolymus hispanicus* L.: Kinetics, equilibrium and thermodynamics. *J. Taiwan Inst. Chem. Eng.* **2011**, *42*, 320–326. [CrossRef]
10. Islam, A.; Ahmad, A.; Laskar, M.A. Characterization of a Chelating Resin Functionalized via Azo Spacer and Its Analytical Applicability for the Determination of Trace Metal Ions in Real Matrices. *J. Appl. Polym. Sci.* **2011**, *123*, 3448–3458. [CrossRef]
11. Ejhieh, N.; Khorsandi, M. Photodecolorization of Eriochrome Black T using NiS-P zeolite as a heterogeneous catalyst. *J. Hazard. Mater.* **2010**, *176*, 629–637. [CrossRef]
12. Yaqoob, A.; Noor, N.H.M.; Serrà, A.; Ibrahim, M.N.M. Advances and challenges in developing efficient graphene oxide-based ZnO photocatalysts for dye photo-oxidation. *Nanomaterials* **2020**, *10*, 932. [CrossRef]
13. Badawi, K.; Ismail, B.; Baaloudj, O.; Abdalla, K.Z. Advanced wastewater treatment process using algal photo-bioreactor associated with dissolved-air flotation system: A pilot-scale demonstration. *J. Water Process. Eng.* **2022**, *46*, 102565. [CrossRef]
14. Ahmad, A.; Hameed, B. Fixed-bed Adsorption of Reactive Azo Dye onto Granular Activated Carbon Prepared from Waste. *J. Hazard. Mater.* **2009**, *175*, 298–303. [CrossRef]
15. Idris, M.O.; Kim, H.C. Exploring the effectiveness of microbial fuel cell for the degradation of organic pollutants coupled with bio-energy generation. *Sustain. Energy Technol. Assess.* **2022**, *52*, 102183.
16. Crini, G. Non-conventional low-cost adsorbents for dye removal: A review. *Bioresour. Technol.* **2006**, *97*, 1061–1085. [CrossRef]
17. Yaqoob, A.A.; Parveen, T.; Umar, K.; Ibrahim, M.N.M. Role of Nanomaterials in the Treatment of Wastewater: A Review. *Water* **2020**, *12*, 495. [CrossRef]
18. Yaqoob, A.; Noor, N.H.M.; Umar, K.; Adnan, R.; Rashid, M. Graphene oxide–ZnO nanocomposite: An efficient visible light photocatalyst for degradation of rhodamine B. *Appl. Nanosci.* **2021**, *11*, 1291–1302. [CrossRef]
19. García-Montaño, J.; Ruiz, N.; Muñoz, I.; Domènech, X.; García-Hortal, J.A.; Torrades, F.; Peral, J. Environmental assessment of different photo-Fenton approaches for commercial reactive dye removal. *J. Hazard. Mater.* **2006**, *138*, 218–225. [CrossRef]
20. Hussein, F.H. Comparison between solar and artificial photocatalytic decolorization of textile industrial wastewater. *Int. J. Photoenergy* **2012**, *2012*, 793648. [CrossRef]
21. Chong, M.N.; Jin, B.; Chow, C.W.K.; Saint, C. Recent developments in photocatalytic water treatment technology: A review. *Water Res.* **2010**, *44*, 2997–3027. [CrossRef] [PubMed]
22. Lachheb, H.; Puzenat, E.; Houasetal, A. Photocatalyticdegradation of various types of dyes (Alizarin S, Crocein Orange G, Methyl Red, Congo Red, Methylene Blue) in water by UV irradiated titania. *Appl. Catal. B Environ.* **2002**, *39*, 75–90. [CrossRef]
23. Zhang, Q.; Jing, Y.H.; Shiue, A.; Chang, C.T.; Chen, B.Y.; Hsueh, C.C. Deciphering effects of chemical structure on azo dye decolorization/degradation characteristics: Bacterial vs. photocatalytic method. *J. Taiwan Inst. Chem. Eng.* **2012**, *43*, 760–766. [CrossRef]
24. Hsueh, C.; Chen, B.Y. Comparative study on reaction selectivity of azo dye decolorization by Pseudomonas luteola. *J. Hazard. Mater.* **2007**, *141*, 842–849. [CrossRef] [PubMed]
25. McCullagh, C.; Skillen, N.; Adams, M.; Robertson, P.K. Photocatalytic reactors for environmental remediation: A review. *J. Chem. Technol. Biotechnol.* **2011**, *86*, 1002–1017. [CrossRef]
26. Chan, S.H.S.; Wu, T.Y.; Juan, J.C.; Teh, C.Y. Recent developments of metal oxide semiconductors as photocatalysts in advanced oxidation processes (AOPs) for treatment of dye waste-water. *J. Chem. Technol. Biotechnol.* **2011**, *86*, 1130–1158. [CrossRef]
27. Guo, M.Y.; Ng, A.M.C.; Liu, F.; Djurisic, A.B.; Chan, W.K. Photocatalytic activity of metal oxides-the role of holes and OH radicals. *Appl. Catal. B Environ.* **2011**, *107*, 150–157. [CrossRef]
28. Fenoll, J.; Hellin, P.; Mart, C.M.; Flores, P.; Navarro, S. Semiconductor oxides-sensitized photodegradation of fenamiphos in leaching water under natural sun light. *Appl. Catal. B Environ.* **2012**, *115–116*, 31–37. [CrossRef]
29. Abualnaja, K.M.; Alprol, A.E.; Abu-Saied, M.A.; Ashour, M.; Mansour, A.T. Removing of anionic dye from aqueous solutions by adsorption using of multiwalled carbon nanotubes and poly (Acrylonitrile-styrene) impregnated with activated carbon. *Sustainability* **2021**, *13*, 7077. [CrossRef]
30. Krifka, S.; Spagnuolo, G.; Schmalz, G.; Schweikl, H. A review of adaptive mechanisms in cell responses towards oxidative stress caused by dental resin monomers. *Biomaterials* **2013**, *34*, 4555–4563. [CrossRef]

31. Liu, J.; Qiao, S.; Liu, H.; Chen, J.; Orpe, A.; Zhao, D.; Lu, G. Extension of the Stober Method to the Preparation of Monodisperse Resorcinol-Formaldehyde Resin Polymer and Carbon Spheres. *Angew. Chem. Int. Ed.* **2011**, *50*, 5947–5951. [CrossRef]
32. Yang, P.; Xu, Q.; Jin, S.; Zhao, Y.; Lu, Y.; Xu, X.; Yu, S. Synthesis of Multifunctional Ag@Au@Phenol Formaldehyde Resin Particles Loaded with Folic Acids for Photothermal Therapy. *Chem. Eur. J.* **2012**, *18*, 9294–9299. [CrossRef]
33. Deng, S.; Lei, J.; Yao, X.; Huang, Y.; Lin, D.; Ju, H. Electrocatalytic reduction of coreactant by highly loaded dendrimer-encapsulated palladium nanoparticles for sensitive electrochemiluminescent immunoassay. *Chem. Commun.* **2012**, *48*, 9159–9161. [CrossRef]
34. Ma, C.; Song, Y.; Shi, J.; Zhang, D.; Guo, Q.; Liu, L. Preparation and electrochemical performance of heteroatom-enriched electrospun carbon nanofibers from melamine formaldehyde resin. *J. Colloid Interface Sci.* **2013**, *395*, 217–223. [CrossRef]
35. Muylaert, I.; Borgers, M.; Bruneel, E.; Schaubroeck, J.; Verpoort, F.; Voort, P.V.D. Ultra stable ordered mesoporous phenol/formaldehyde polymers as a heterogeneous support for vanadium oxide. *Chem. Commun.* **2008**, *37*, 4475–4477. [CrossRef]
36. Zhao, M.; Song, H. Catalytic Graphitization of Phenolic Resin. *J. Mater. Sci. Technol.* **2011**, *27*, 266–270. [CrossRef]
37. Zhao, J.; Niu, W.; Zhang, L.; Cai, H.; Han, M.; Yuan, Y.; Majeed, S.; Anjum, S.; Xu, G. A Template-Free and Surfactant-Free Method for High-Yield Synthesis of Highly Monodisperse 3-Aminophenol-Formaldehyde Resin and Carbon Nano/Microspheres. *Macromolecules* **2013**, *46*, 140–145. [CrossRef]
38. Mori, K.; Dojo, M.; Yamashita, H. Pd and Pd-Ag Nanoparticles within a Macroreticular Basic Resin: An Efficient Catalyst for Hydrogen Production from Formic Acid Decomposition. *ACS Catal.* **2013**, *3*, 1114–1119. [CrossRef]
39. Wu, Y.; Li, Y.; Qin, L.; Yang, F.; Wu, D. Monodispersed or narrow-dispersed melamine–formaldehyde resin polymer colloidal spheres: Preparation, size-control, modification, bioconjugation and particle formation mechanism. *J. Mater. Chem. B* **2013**, *1*, 204–212. [CrossRef]
40. He, X.H.; Wu, X.M.; Cai, X.; Lin, S.L.; Xie, M.R.; Zhu, X.Y.; Yan, D.Y. Functionalization of Magnetic Nanoparticles with Dendritic–Linear–Brush-Like Triblock Copolymers and Their Drug Release Properties. *Langmuir* **2012**, *28*, 11929–11938. [CrossRef]
41. Wang, Y.Q.; Zou, B.F.; Gao, T.; Wu, X.P.; Lou, S.Y.; Zhou, S.M. Constructing carbon-coated $Fe_3O_4$ hierarchical microstructures with a porous structure and their excellent Cr(VI) ion removal properties. *J. Mater. Chem.* **2012**, *22*, 9034–9040. [CrossRef]
42. Matsuno, R.; Yamamoto, K.; Otsuka, H.; Takahara, A. Polystyrene-Grafted Magnetite Nanoparticles Prepared through Surface-Initiated Nitroxyl-Mediated Radical Polymerization. *Chem. Mater.* **2003**, *15*, 3–5. [CrossRef]
43. Zhang, H.; Zhong, X.; Xu, J.J.; Chen, H.Y. $Fe_3O_4$/Polypyrrole/Au Nanocomposites with Core/Shell/Shell Structure: Synthesis, Characterization, and Their Electrochemical Properties. *Langmuir* **2008**, *24*, 13748–13752. [CrossRef] [PubMed]
44. Zhang, C.; Wang, Y.; Zhang, X.; Guo, H. $Fe_{78}Si_9B_{13}$ amorphous alloys for the decolorization process of azo dye aqueous solutions with different initial concentrations at different reaction temperatures. *Vacuum* **2020**, *176*, 109301. [CrossRef]
45. Qiao, J.-H.; Chen, K.; Li, S.-J.; Liu, Y.-C.; Cao, H.-W.; Wei, G.; Kong, L.-P.; Zhang, X.; Liu, H.-T. Plasma spray-chemical vapor deposition of nanotextured film with α/β $Bi_2O3$ heterostructure and photocatalytic degradation performance. *Vacuum* **2021**, *188*, 110206. [CrossRef]
46. Parida, D.; Moreau, E.; Nazir, R.; Salmeia, K.A.; Friston, R.; Zhao, R.; Lehner, S.; Jovic, M.; Gann, S. Smart hydrogel-microsphere embedded silver nanoparticle catalyst with high activity and selectivity for the reduction of 4-nitrophenol and azo dyes. *J. Hazard. Mat.* **2021**, *416*, 126237. [CrossRef]
47. Kong, L.R.; Lu, X.F.; Jin, E.; Jiang, S.; Bian, X.J.; Zhang, W.J.; Wang, C. Accurately Tuning the Dispersity and Size of Palladium Particles on Carbon Spheres and Using Carbon Spheres/Palladium Composite as Support for Polyaniline in $H_2O_2$ Electrochemical Sensing. *Langmuir* **2010**, *26*, 5985–5990. [CrossRef]
48. Xuan, S.H.; Wang, Y.X.J.; Leung, K.C.F.; Shu, K.Y. Synthesis of $Fe_3O_4$@Polyaniline Core/Shell Microspheres with Well-Defined Blackberry-Like Morphology. *J. Phys. Chem. C* **2008**, *112*, 18804–18889. [CrossRef]
49. Milyutin, V.V.; Mikheev, S.V.; Gelis, V.M.; Kozlitin, E.A. Sorption of Cesium on Ferrocyanide Sorbents from Highly Saline Solutions. *Radiochemistry* **2009**, *51*, 298–300. [CrossRef]
50. Zicman, L.R.; Neacsu, E.; Done, L.; Tugulan, L.; Dragolici, F.; Obreja, B.T.; Dobre, T. Removal of 137Cs ions from aqueous radioactive waste using nickel ferrocyanide, precipitated on silica gel. *Bull. Rom. Chem. Eng. Soc.* **2015**, *2*, 84–99.
51. Nilchi, A.; Atashi, H.; Javid, A.H.; Saberi, R. Preparations of PAN-Based Adsorbers for Separation of Cesium and Cobalt from Radioactive Wastes. *Appl. Radiat. Isot.* **2007**, *65*, 482–487. [CrossRef] [PubMed]
52. Kozlov, P.V.; Kazadaev, A.A.; Makarovskii, R.A.; Remizov, M.B.; Verbitskii, K.V.; Logunov, M.V. Development of a Process for Cesium Recovery from the Clarified Phase of High-Level Waste Storage Tanks of the Mayak Production Association with a Ferrocyanide Sorbent. *Radiochemistry* **2016**, *58*, 295–301. [CrossRef]
53. Milyutin, V.V.; Gelis, V.M.; Ershov, B.G.; Seliverstov, A.F. Effect of Complexing Agents and Surfactants on Coprecipitation of Cesium Radionuclides with Nickel Ferrocyanide. *Radiochemistry* **2011**, *50*, 67–69. [CrossRef]
54. Milyutin, V.V.; Zelenin, P.G.; Kozlov, P.V.; Remizov, M.B.; Kondrutskii, D.A. Sorption of Cesium from Alkaline Solutions onto Resorcinol-Formaldehyde Sorbents. *Radiochemistry* **2019**, *61*, 714–718. [CrossRef]
55. Brown, G.N.; Russell, R.L.; Peterson, R.A. *Small-Column Cesium Ion Exchange Elution Testing of Spherical Resorcinol-Formaldehyde*; Pacific Northwest National Laboratory: Richland, WA, USA, 2011.
56. Hubler, T.L.; Franz, J.A.; Shaw, W.J.; Bryan, S.; Hallen, R.; Brown, G.N.; Bray, L.A.; Linehan, J.C. *Synthesis, Structural Characterization, and Performance Evaluation of Resorcinol-Formaldehyde (RF) Ion-Exchange Resin*; Pacific Northwest Laboratory: Richland, WA, USA, 1995.
57. Hubler, T.L.; Shaw, W.J.; Brown, G.N.; Linehan, J.C.; Franz, J.A.; Hart, T.R.; Hogan, M.O. *Chemical Derivation to Enhance the Chemical/Oxidative Stability of Resorcinol-Formaldehyde (R-F) Resin*; Pacific Northwest National Lab.: Richland, WA, USA, 1996.

58. Taguchi, S.; Nakatani, T.; Saeki, H.; Tayakout-Fayolle, M.; Itoh, K.; Yamamoto, T. Characterization of Resorcinol–Formaldehyde Hydrogel as Adsorbent for Cesium Ion. *Adsorption* **2021**, *27*, 81–90. [CrossRef]
59. Aquino, C.M.; Costero, A.M.; Gil, S.; Gavina, P. Resorcinol Functionalized Gold Nanoparticles for Formaldehyde Colorimetric Detection. *Nanomaterials* **2019**, *9*, 302. [CrossRef]
60. Gupta, V.K. Suhas Application of low-cost adsorbents for dye removal—A review. *J. Environ. Manag.* **2009**, *90*, 2313–2342. [CrossRef]
61. Alkan, M.; Demirbas, O.; Celikcapa, S.; Dogan, M. Sorption of Acid Red 57 from Aqueous Solutions onto Sepiolite. *J. Hazard. Mater.* **2004**, *116*, 135–145. [CrossRef]
62. Turhan, K.; Ozturkcan, S.A. Decolorization and Degradation of Reactive Dye in Aqueous Solution by Ozonation in a Semi-Batch Bubble Column Reactor. *Water Air Soil Pollut.* **2012**, *224*, 1353. [CrossRef]
63. Abdallah, R.; Taha, S. Biosorption of methylene blue from aqueous solution by nonviable Aspergillus fumigates. *Chem. Eng. J.* **2012**, *195*, 69–76. [CrossRef]
64. Wang, B.E.; Hu, Y.Y. Comparison of four supports for adsorption of reactive dyes by immobilized Aspergillus fumigatus beads. *J. Environ. Sci.* **2007**, *19*, 451–457. [CrossRef]
65. Wainwright, M.; Crossley, K.B. Methylene Blue-a therapeutic dye for all seasons? *J. Chemother.* **2002**, *14*, 431–443. [CrossRef]
66. Frankenburg, F.R.; Baldessarini, R.J. Neurosyphilis, Malaria, and the Discovery of Antipsychotic Agents. *Harv. Rev. Psychiatry* **2008**, *16*, 299–307. [CrossRef]
67. Chung, K.T.; Stevens, S.E. Degradation azo dyes by environmental microorganisms and helminths. *Environ. Toxicol. Chem.* **1993**, *12*, 2121–2132. [CrossRef]
68. Aksu, Z.; Tezer, S. Equilibrium and Kinetic Modelling of Biosorption of Remazol Black B by *Rhizopus arrhizus* in a Batch System: Effect of Temperature. *Process Biochem.* **2000**, *36*, 431–439. [CrossRef]
69. Lucas, M.S.; Peres, J.A. Decolorization of the Azo Dye Reactive Black 5 by Fenton and Photo Fenton Oxidatio. *Dyes Pigm.* **2006**, *71*, 236–244. [CrossRef]
70. Albert, M.; Lessin, M.S.; Gilchrist, B.F. Methylene blue: Dangerous dye for neonates. *J. Pediatr. Surg.* **2003**, *38*, 1244–1245. [CrossRef]
71. Srinivasan, M.; White, T. Degradation of Methylene Blue by Three-Dimensionally Ordered Macroporous Titania. *Environ. Sci. Technol.* **2007**, *41*, 4405–4409. [CrossRef]
72. Zhang, Y.G.; Ma, L.L.; Li, J.L.; Yu, Y. In Situ Fenton Reagent Generated from $TiO_2/Cu_2O$ Composite Film: A New Way to Utilize $TiO_2$ under Visible Light Irradiation. *Environ. Sci. Technol.* **2007**, *41*, 6264–6269. [CrossRef]
73. Bielska, M.; Szymanowski, J. Removal of methylene blue from waste water using micellar enhanced ultrafiltration. *Water Res.* **2006**, *40*, 1027–1033. [CrossRef]
74. Hameed, B.H.; Ahmad, A.L.; Latiff, K.N.A. Adsorption of basic dye (methylene blue) onto activated carbon prepared from rattan sawdust. *Dyes Pigm.* **2007**, *75*, 143–149. [CrossRef]
75. Zhang, S.; Fan, Q.; Gao, H.; Huang, Y.; Liu, X.; Li, J.; Xu, X.; Wang, X. Formation of $Fe_3O_4$@$MnO_2$ ballin-ball hollow spheres as a high performance catalyst with enhanced catalytic performances. *J. Mater. Chem. A* **2016**, *4*, 1414–1422. [CrossRef]
76. Wang, Y.; Pan, F.; Dong, W.; Xu, L.; Wu, K.; Xu, G.; Chen, W. Recyclable silver-decorated magnetic titania nanocomposite with enhanced visible-light photocatalytic activity. *Appl. Catal. B Environ.* **2016**, *189*, 192–198. [CrossRef]
77. Gawande, M.B.; Branco, P.S.; Varma, R.S. Nano-magnetite ($Fe_3O_4$) as support for recyclable nanocatalysts in the development of sustainable methodologies. *Chem. Soc. Rev.* **2013**, *42*, 3371–3393. [CrossRef]
78. Varma, R.S. Journey on greener pathways: From the use of alternate energy inputs and benign reaction media to sustainable applications of nano-catalysts in synthesis and environmental remediation. *Green Chem.* **2014**, *16*, 2027–2041. [CrossRef]
79. Sharma, V.K. Festschrift in Honor of Rajender S. Varma. *ACS Sustain. Chem. Eng.* **2016**, *4*, 640–642. [CrossRef]
80. Baig, R.B.N.; Varma, R.S. Organic synthesis via magnetic attraction: Benign and sustainable protocols using magnetic nanoferrites. *Green Chem.* **2013**, *15*, 398–417. [CrossRef]
81. Atarod, M.; Nasrollahzadeh, M.; Sajadi, S.M. Green synthesis of Pd/RGO/$Fe_3O_4$ nanocomposite using Withania coagulans leaf extract and its application as magnetically separable and reusable catalyst for the reduction of 4-nitrophenol. *J. Colloid Interface Sci.* **2016**, *465*, 249–258. [CrossRef]
82. Sajadi, S.M.; Nasrollahzadeh, M.; Maham, M. Aqueous extract from seeds of Silybum marianum L. as a green material for preparation of the Cu/$Fe_3O_4$ nanoparticles: A magnetically recoverable and reusable catalyst for the reduction of nitroarenes. *J. Colloid Interface Sci.* **2016**, *469*, 93–98. [CrossRef]
83. Veremchuk, I.; Antonyshyn, I.; Candolfi, C.; Feng, X.; Burkhardt, U.; Baitinger, M.; Zhao, J.-T.; Grin, Y. Diffusion-Controlled Formation of $Ti_2O_3$ during Spark-Plasma Synthesis. *Inorg. Chem.* **2013**, *52*, 4458–4463.
84. Yang, K.; Peng, H.B.; Wen, Y.H.; Li, N. Re-examination of characteristic FTIR spectrum of secondary layer in bilayer oleic acid-coated $Fe_3O_4$ nanoparticles. *Appl. Surf. Sci.* **2010**, *256*, 3093–3097. [CrossRef]
85. Lasperas, M.; Llorett, T.; Chaves, L.; Rodriguez, I.; Cauvel, A.; Brunel, D. Amine functions linked to MCM-41-type silicas as a new class of solid base catalysts for condensation reactions. *Stud. Surf. Sci. Catal.* **1997**, *108*, 75–82. [CrossRef]
86. Allen, D.J.; Ishida, H. Synthesis and properties of polybenzoxazines containing pyridyl group. *Polymer* **2007**, *48*, 6763–6772. [CrossRef]

87. Chernykh, I.; Liu, J.P.; Ishida, H. Synthesis and properties of a new crosslinkable polymer containing benzoxazine moiety in the main chain. *Polymer* **2006**, *47*, 7664–7669. [CrossRef]
88. Ma, Z.Y.; Guan, Y.P.; Liu, H.Z. synthesis and characterization of micron-sized monodisperse superparamagnetic polymer particles with amino groups. *J. Polym. Sci. Part A Polym. Chem.* **2005**, *43*, 3433–3439. [CrossRef]
89. Ramanathan, T.; Fisher, F.T.; Ruoff, R.S.; Brinson, L.C. Amino-functionalized carbon nanotubes for binding to polymers and biological systems. *Chem. Mater.* **2005**, *17*, 1290–1295. [CrossRef]
90. Morlieras, J.; Chezal, J.-M.; Miot-Noirault, E.; Roux, A.; Heinrich-Balard, L.; Cohen, R.; Tarrit, S. Development of gadolinium based nanoparticles having an affinity towards melanin. *Nanoscale* **2013**, *5*, 1603–1615. [CrossRef]
91. Jahagirdar, S.S.; Shrihari, S.; Manu, B. Reuse of incinerated textile mill sludge as adsorbent for dye removal. *KSCE J. Civ. Eng.* **2015**, *19*, 1982–1986. [CrossRef]
92. Rehman, M.S.U.; Kim, I.; Rashid, N.; Umer, M.A.; Sajid, M.; Han, J.I. Adsorption of Brilliant Green Dye on Biochar Prepared From Lignocellulosic Bioethanol Plant Waste. *Clean Soil Air Water* **2016**, *44*, 55–62. [CrossRef]
93. Laskar, N.; Kumar, U. Removal of Brilliant Green dye from water by modified Bambusa Tulda: Adsorption isotherm, kinetics and thermodynamics study. *Int. J. Environ. Sci. Technol.* **2018**, *16*, 1649–1662. [CrossRef]
94. Moeinpour, F.; Alimoradi, A.; Kazemi, M. Efficient removal of Eriochrome black-T from aqueous solution using $NiFe_2O_4$ magnetic nanoparticles. *J. Environ. Health Sci. Eng.* **2014**, *12*, 112. [CrossRef] [PubMed]
95. Khalid, A.; Zubair, M.; Ihsanullah, A. A Comparative Study on the Adsorption of Eriochrome Black T Dye from Aqueous Solution on Graphene and Acid-Modified Graphene. *Arab. J. Sci. Eng.* **2018**, *43*, 2167–2179. [CrossRef]
96. Fayoud, N.; Tahiri, S.; Younssi, S.A.; Albizane, A.; Gallart-Mateu, D.; Cervera, M.L.; De la Guardia, M. Kinetic, isotherm and thermodynamic studies of the adsorption of methylene blue dye onto agro-based cellulosic materials. *Desalination Water Treat.* **2016**, *57*, 16611–16625. [CrossRef]
97. Baidya, K.S.; Kumar, U. Adsorption of brilliant green dye from aqueous solution onto chemically modified areca nut husk. *Afr. J. Chem. Eng.* **2021**, *35*, 33–43. [CrossRef]
98. Salman, S.M.; Ali, A.; Khan, B.; Iqbal, M.; Alamzeb, M. Thermodynamic and kinetic insights into plant-mediated detoxification of lead, cadmium, and chromium from aqueous solutions by chemically modified Salvia moorcroftiana leaves. *Environ. Sci. Pollut. Res. Int.* **2019**, *26*, 14339–14349. [CrossRef]
99. Mane, V.S.; Babu, P.V.V. Studies on the adsorption of Brilliant Green dye from aqueous solution onto low-cost NaOH treated saw dust. *Desalination* **2011**, *273*, 321–329. [CrossRef]
100. Auta, M.; Hameed, B.H. Modified mesoporous clay adsorbent for adsorption isotherm and kinetics of methylene blue. *Chem. Eng. J.* **2012**, *198–199*, 219–227. [CrossRef]
101. Mattson, J.S.M.H.B. *Activated Carbon: Surface Chemistry and Adsorption from Solution*; M. Dekker: New York, NY, USA, 1971.
102. Rashidi, R.; Khaniabadi, Y.O.; Ghaderpoori, M. Adsorption of Eriochrome black-T from aqueous environment by raw Montmorillonite. *Int. J. Environ. Anal. Chem.* **2021**, 1–15. [CrossRef]